O-Band 50Gb/s Ring Modulator in a 300mm Si Photonic Platform

Audrey Michard, N. Michit, J. F. Carpentier, P. Le Maitre, J. B. Quelene, Pietro Maris Ferreira

O-band 50Gb/s ring modulator in a 300mm Si photonic platform

A. Michard[1,2], N. Michit[1], JF. Carpentier[1], P. Le Maître[1], JB. Quélène[1], P. Maris Ferreira[2]

[1] STMicroelectronics, Crolles, France, audrey.michard@st.com
[2] GeePs, UMR CNRS 8507, CentraleSupélec, Université Paris-Saclay, Gif-sur-Yvette, France

Abstract *A carrier-depletion ring modulator is demonstrated to operate at 50Gb/s in the O-band of optical communications. The high-bandwidth device was designed using an analytical model, taking into account non-linear effects. A 1.9dB extinction ratio is achieved with a 3Vpp driving voltage.*

Introduction

Ring resonator modulators (RRM) are key components for silicon photonics, and especially for very short reach optical interconnects involved in future supercomputers. Indeed RRM offer an attractive solution for Wavelength Division Modulation (WDM) systems since they present a small footprint, a high wavelength selectivity and a low energy consumption. Such ring-based transceiver[1] has been proposed to meet High Performance Computing (HPC) challenges. But bandwidth requirements are expected to grow[2] and we believe that 40-100Gb/s modulators will be adopted in next design. Among the possible modulation junctions, carrier-depletion rings based on a reverse-biased PN diode are shown to be the best configuration to achieve high data rates[3]. Therefore, we present a PN-based RRM to operate at 50Gb/s and beyond.

High-speed RRM have already been demonstrated in the literature[4-6]. However most published silicon modulators have been designed for the C-band of optical links (1530nm – 1570nm). In this paper, we focus on the O-band (near 1310nm), which is strongly used in HPC interconnect area. Lasers efficiency over temperature is better managed in the O-band[7] which is crucial for close opto-electric integration leading to tricky operating conditions. Moreover, the O-band benefits from better confined optical mode, resulting in more compact circuits[7]. To the best of our knowledge, the literature exhibits only two demonstrations of a high-bandwidth RRM operating at roughly 1310nm[8,9], both being fabricated in a 200mm platform. This work reports modelling, fabrication and measurement of ring modulators in a 300mm industrial photonic platform. At 50Gb/s, open eye diagrams are obtained without pre-emphasis, exhibiting a 1.9dB extinction ratio with a 3Vpp driving voltage.

Ring modulator design

The RRM design and its parameters' optimization to achieve a high bandwidth requires the use of a model to simulate its expected behavior. A modelling was developed based on analytical equations that govern PN junction modulation and wave propagation into a ring resonator. Such equations are reported in the literature[3] and are not presented in this paper. The model does not take into account retro-diffusion since high coupling between ring and adjacent waveguide enables to neglect back propagation of light wave. But it includes self-heating effects that appear within the ring when input optical power is increasing. In short, the proposed model enables to predict the influence of modulation and of nonlinearities, such as two-photon absorption, on ring resonances.

From this modelling, two frequency limitations are defined for the RRM: an optical limitation (f_{opt}) due to the cavity photon lifetime and the coupling time; and an electrical limitation (f_{elec}) due to the RC product of the device. Optical and electrical bandwidths are expressed as Eq. (1), where c is the light speed in vacuum, λ_{res} is the resonant wavelength, $\mathbb{Q}$ is the Q-factor, R_j and C_j are the junction resistance and capacitance.

$$f_{opt} = \frac{c}{\lambda_{res}\mathbb{Q}} \quad \& \quad f_{elec} = \frac{1}{2\pi}\frac{1}{R_j C_j} \qquad (1)$$

When optimizing the RRM, it is also important to consider its modulation efficiency and its performance defined as the transmitter penalty. The modulation efficiency is given by the wavelength shift ($\Delta\lambda_{shift}$) with respect to the driving voltage applied to the PN junction. The transmitter penalty (TP) is the image of both extinction ratio ($ER = P_1/P_0$) and insertion losses ($IL = 2P_{in}/(P_1 + P_0)$) and is derived as Eq. (2). P_1 and P_0 are respectively the optical powers for a "1" bit and a "0" bit while P_{in} is the input power injected into the RRM. The optimal modulation wavelength corresponds to the minimal transmitter penalty.

$$TP = IL * \frac{ER + 1}{ER - 1} = \frac{2P_{in}}{P_1 - P_0} \qquad (2)$$

One can note that a trade-off exists between these four parameters. Indeed, the optical bandwidth optimization requires to reduce the Q-factor that means increase losses into the ring, by increasing junction doping concentrations and/or by increasing the coupling. However, increasing

doping concentrations results in a higher junction capacitance and hence a lower electrical bandwidth. Moreover high doping levels generally degrade the transmitter penalty, but enable to improve the phase shift generated by the PN junction, and thus improve the resonance shift. To illustrate these tendencies, we have plotted in Fig. 1 the transmitter penalty and the maximal data rate achievable by the ring with respect to the doping concentrations. Curves are calculated from our analytical model and compared for different coupling coefficients and waveguide widths. The maximal data rate is estimated from the electro-optic bandwidth (f_{-3dB}) described by Eq. (3).

$$\frac{1}{f_{-3dB}^2} = \frac{1}{f_{elec}^2} + \frac{1}{f_{opt}^2} \quad (3)$$

Based on Fig. 1, we have designed a ring resonator likely to perform a 50Gb/s modulation. Its characteristics are given in Tab. 1. Principally two major changes have been introduced, compared with a low-bandwidth ring. First, the slab width between the waveguide and metal contacts has been reduced to decrease the junction resistance and secondly, doping levels have been increased above 10^{18}cm^{-3}. R_j and C_j are estimated to 35Ω and 40fF. A cross-section of the ring waveguide is represented in Fig. 2 (a), showing dimensions and junction's definition.

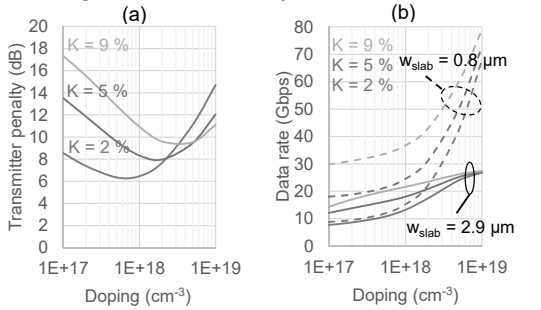

Fig. 1: Simulated ring performance metrics with respect to doping concentrations for various coupling coefficients and slab widths. (a) Transmitter penalty, (b) Maximal data rate.

Ring fabrication

The RRM was fabricated using the silicon photonic platform on 300mm SOI wafers at STMicroelectronics[10]. New implant processes were designed to achieve high junction doping. Moreover the "deep-slab" option was used, meaning that the slab height is reduced to 50nm. A "deep-slab" waveguide enables to increase the light confinement and thus results in a better modulation efficiency[11]. This enables to compensate for the weaker carrier-depletion effect in the O-band than in the C-band.

A microphotograph of the fabricated device is shown in Fig. 2 (b). The RRM has a racetrack form with an 8µm-radius and a 2µm-long coupling section. The gap between the ring and the straight waveguide is set to 230nm to target a 7% power coupling coefficient.

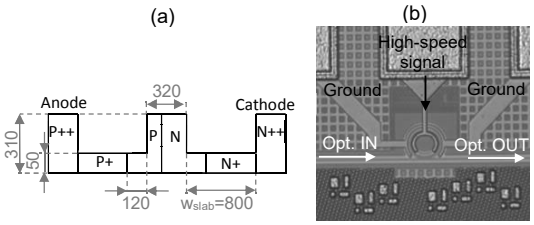

Fig. 2: (a) Schematic cross-section of the ring waveguide including PN junction. Dimensions are given in nm. (b) Microphotograph of the fabricated ring modulator.

Static optical characterization

Static measurements were performed at wavelength ranging from 1300nm to 1330nm, using the Yenista CT400 optical component tester which enables a resolution down to 1pm. The laser power was set to a few microwatts to ensure a linear operating mode of the RRM.

Power transmission spectra are measured at various voltage biases and are illustrated in Fig. 3 (a). $\mathbb{Q}$ is calculated from the measure of the full width at half maximum which is 240pm. Thus, $\mathbb{Q}$ is roughly 5500 which corresponds to an optical bandwidth of 41GHz. Assuming a voltage swing between 0 and -2V, the wavelength shift is 20pm/V. This value can be converted into the classical product $V_\pi L_\pi$ of the junction and is 1.02V-cm.

The RRM modulation efficiency was also measured at wafer-level across 26 dies, resulting in a statistics of 104 samples (4 resonances were studied per ring). Fig. 3 (b) reports boxplot of $\Delta\lambda_{shift}$ variations and shows a mean of 19.8pm/V with a standard deviation of 1.7pm/V. The peak shift exhibits a low deviation thanks to the 300mm process performance.

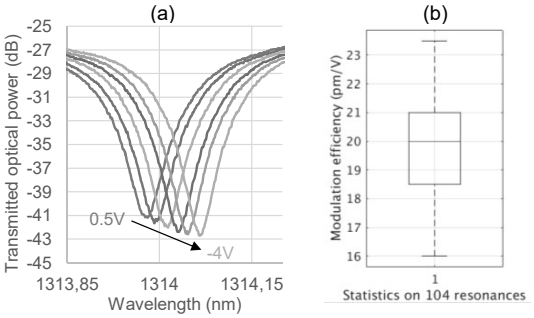

Fig. 3: (a) Transmission spectra of ring resonator for different driving voltages (0.5V, 0V, -1V, -2V, -3, and -4V). (b) Modulation efficiency measured across 26 dies.

For a modulation voltage from 0V to -4V, we derive the transmitter penalty of the modulator according to Eq. (2). The TP spectrum is illustrated in Fig. 4 (a) and is minimum (8.15dB) at 1313.957nm. The wavelength tuning should

center on a 75pm-wide range to keep the TP degradation below 1dB.

Finally the RRM non-linear behavior was analyzed and compared to our analytical model. Fig. 4 (b) displays transmission spectra for increasing input power. Such asymmetric resonances are characteristic of self-heating effects and are well fitted by the model. In a HPC WDM interconnection, RRM input power will be however kept below 250µW, ensuring that non-linear phenomena can be neglected.

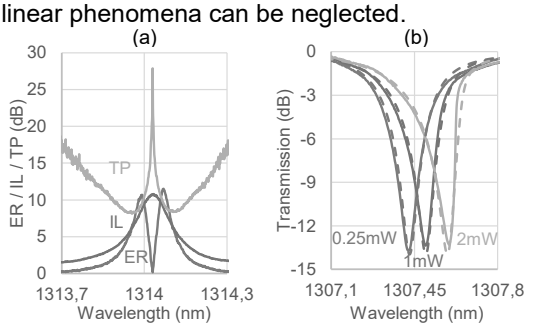

Fig. 4: (a) ER, IL, and TP spectra for a modulation between 0V and -4V bias. (b) Transmission spectra under 0V-bias for different input powers. Solid lines are measurement results while dashed lines are obtained with our model.

High-speed performance

High-speed measurements were performed using a Keysight BERT M9505A for pattern generation associated with a Keysight DCA-X 86100D sampling oscilloscope for optical eye diagram inspection. The electrical pattern is amplified and added to a DC bias through a bias tee to drive the RRM at the desired operating point. A 50Ω resistance is integrated in parallel to the device to avoid reflections to the amplifier.

(a) 20Gbps, 1314.970nm, 1.5Vpp biased at 0Vdc ER = 2.01 dB

(b) 50Gbps, 1314.020nm, 3Vpp biased at -2Vdc ER = 1.90 dB

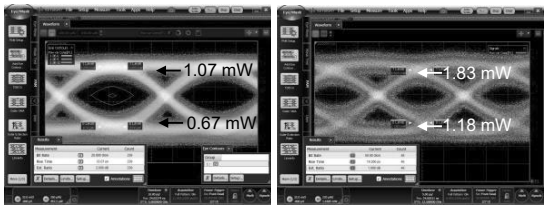

Fig. 5: Eye diagrams of the ring modulator for different operating conditions.

Open eye diagrams are obtained and are illustrated in Fig. 5. Measurements have been performed using a 2^7-1 non-return-to-zero pseudo random bit sequence. No pre-emphasis signal was used. Eye diagram is shown at 20Gb/s at 1.5Vpp driving voltage under 0V-bias (Fig. 5 (a)). An extinction ratio of 2.0dB and a BER contour of 10^{-9} are achieved. The small CMOS-compatible voltage ensures a low-power operation required for HPC applications. Eye diagram is also shown at 50Gb/s (Fig. 5 (b)) but the driving swing has been increased to 3Vpp to compensate for larger inter-symbol interferences. With a 2V-reverse bias, the ER is 1.9dB.

The electro-optic bandwidth f_{-3dB} is estimated to 36GHz, meaning that the RRM is limited by its optical bandwidth due to cavity photon lifetime. Further works will focus on RRM improvement to reduce the driving swing at high-speed. An in-depth design of ring waveguide to reduce the rib height will be considered to increase the modulation efficiency, provided that changes are acceptable with 300mm platform.

Conclusions

In this paper, we have reported a RRM in a 300mm silicon photonics platform operating in the O-band up to 50Gb/s without pre-emphasis. Good results in terms of modulation efficiency and eye diagrams generation have been demonstrated. Further RRM design and process optimization, like the use of immersion lithography, will enable to enhance RRM global performance.

Tab. 1: Summary of ring's parameters and performance

Dimensions	Doping (cm^{-3})	Static performance	Dynamic performance
Radius = 8µm	$N = 3\times10^{18}$	FSR = 7.5nm	f_{-3dB} = 36 GHz
Coupling length = 2µm	$P = 5\times10^{18}$	Peak depth = 15 dB	ER = 1.9 dB
Gap = 230nm	$N+ = 5\times10^{19}$	Q-factor = 5500	
	$P+ = 5\times10^{19}$	$\Delta\lambda_{shift}$ = 20 pm/V	

Acknowledgements

The authors are grateful to Nathalie Vulliet, with STMicroelectronics, who was responsible of the ring process integration. The authors would like to thank also the CEA LETI for their optical characterization bench, and Philippe Grosse for his assistance in the measurement.

References

[1] Y. Thonnart et al., ISSCC Dig. Tech., paper 21.4, p. 350 (2018)
[2] S. Rumley et al., Parallel Computing, Vol. 64, p. 65 (2017)
[3] O. Dubray et al., J. Selected Topics in Quantum Electronics, Vol. **22**, no. 6, p. 89 (2016)
[4] T. Baba et al., Opt. Exp., Vol. **21**, no. 10, p. 11869 (2013)
[5] M. Pantouvaki et al., Proc. ECOC, ID 0631 (2015)
[6] M. Pantouvaki et al., J. Lightwave Technol., Vol. **35**, no. 4, p. 631 (2017)
[7] C. Cole, 5th Int. Symp. for Opt. Interconnect in Data Center, ECOC (2017)
[8] Z. Xuan et al., Opt. Exp., Vol. **22**, no. 23, p. 28284 (2014)
[9] J. Van Campenhout et al., Proc. OFC, W1I.1 (2018)
[10] P. Le Maître et al., Proc. ECOC, ID 0448 (2015)
[11] D. Perez-Galacho et al., Opt. Exp., Vol. **25**, no. 10, p. 11217 (2017)